BULLETIN OF THE POLISH ACADEMY OF SCIENCES
TECHNICAL SCIENCES, Vol. 72(4), 2024, Article number: e150110
DOI: 10.24425/bpasts.2024.150110

Analysis of the influence of karst cave parameters on surface settlement in TBM tunnelling

Bichang DONG[1], Tao YANG[1]*, Binbin JU[1], Zhongying QU[2], and Chao YI[3]

[1] School of Transportation and Logistics Engineering, Wuhan University of Technology, Wuhan Hubei 430063, China
[2] Wuhan Municipal Engineering Design and Research Institute Co., Ltd. Wuhan Hubei 430063, China
[3] China Railway Seven Bureau Group Fourth Engineering Co., Ltd. Wuhan 430200, China

Abstract. In order to study the influence of multiple karst cave factors on surface settlement during tunnel boring machine (referred to TBM hereinafter) tunnelling, a three-dimensional numerical model is built by taking a subway project as an example and combining it with MIDAS GTS NX finite element software. Secondly, the influence of the radius, height, angle, vertical net distance and horizontal distance of the karst cave on maximum surface settlement is studied and sorted under the two working conditions of treatment and lack of treatment using the gray correlation analysis method. Additionally, a multi-factor numerical model of the untreated karst cave is established. Finally, based on the preceding research, a multi-factor prediction model for maximum surface settlement is proposed and tested. The results reveal that when the karst cave is not treated, the radius and height of the karst cave have a significant effect on maximum surface settlement. Following cave treatment however, the influence of the cave parameters on maximum settlement of the surface is greatly reduced. The calculating model created in this study offers excellent prediction accuracy and good adaptability.

Keywords: karst cave; TBM tunnelling; surface subsidence; gray correlation analysis; MIDAS.

1. INTRODUCTION

In recent years, TBM tunnelling has been widely used in underground engineering due to its safety and efficiency, low influence on the surrounding environment and high automation. However, in the process of construction, numerous challenging geological conditions are regularly encountered, and karst is one of them that has a tremendous impact on the projects in question [1]. The study by Guo Chunqing *et al.* [2] shows that, according to the distribution area of strata containing soluble rocks, the area of the karst region in China exceeds 3.444 million km^2, which is 1/3 of the country's geographical area. In Wuhan, for example, there are karst distributions along almost the whole line of some rail transit routes. The impact of karst on tunnels is mainly manifested in the deformation and destabilization of the tunnel periphery, which often leads to local collapse, falling blocks, falling rocks, shield headers, etc. during tunnel excavation, and in turn greatly affects the progress of construction and safety of the machinery, even jeopardizing the personal safety of the construction personnel [3–8]. Therefore, for tunnel construction in the karst development area, it is of considerable theoretical and practical value to analyze the influence of caves on its construction.

During construction of a shield tunnel, different types of caves will produce varying degrees of impact on the construction and need to be analyzed and treated with different methods. At present, the most generally utilized research method is numerical simulation. Tan Daiming *et al.* [9] used FLAC3D software to simulate and calculate the influence of lateral voids on the stability of surrounding rocks in karst tunnels. Based on MIDAS GTS software, Yi Jiemin [10] researched the influence law of different locations and sizes of caves on the stability of tunnels and the internal force in tunnel lining. Based on FLAC3D software, Mo Yangchun *et al.* [11] conducted a numerical simulation of the deformation characteristics of the surrounding rock containing caverns in the side of the tunnel, and analyzed the influence of different distances and sizes of caverns on the deformation of the rock. By using the MIDAS GTS program, Liu Daoyan *et al.* [12] conducted a study on the impact of various factors, including the location, radius, filling status and spacing of cavern tunnels during the excavation of the Kunming Railway No. 4 line. Fang Z.D. *et al.* [13] used Solid Works modelling software to build the shield machine model, then constructed a discrete element model of the karst stratum by calibrating the discrete element EDEM fine view parameters. Simulation of the shield tunnelling process under varied karst cave filling strengths was realized. The influence of the ratio of the karst cave filling strength to the strength of the surrounding rock on the stability of the surrounding rock was explored.

As can be seen above, numerous academics have carried out extensive research on tunnel construction in karst areas based on diverse engineering projects, and they have achieved plentiful research results. However, due to the complexity of karst geology, there are still many difficulties that demand in-depth examination, such as the regional features of karst geology, the influence of shield tunnelling in karst geology on the environment, and so on. This paper takes a karst section of the Wuhan

*e-mail: yang-tao@whut.edu.cn

Manuscript submitted 2023-10-16, revised 2024-03-11, initially accepted for publication 2024-03-18, published in July 2024.

subway project as an example, combining the MIDAS GTS software and mathematical physics method, to study the influence of the cavern parameters on maximum ground settlement and to put forward the prediction model of ground settlement during TBM tunnelling, in order to provide references for the theoretical research, design and construction of shield tunnels in subsequent karst development areas.

2. PROJECT OVERVIEW

The subway project in Wuhan is located in the southern part of the city, with a total length of 16.9 km, all of which are underground tunnels with 7 stations along the line. The depth of the tunnel crown is about 5 m at the shallowest point and 30 m at the deepest point, which is mainly constructed by means of TBM tunnelling, and partially constructed by the open cut or mining method. The selected segment is 162 m long (CK40+619.25–CK40+781.25) and forms part of the Jiang Tan project. The cross-section is circular, with a diameter of 6.2 m, the tunnel lining thickness of 0.35 m and a ring width of 1.5 m, with C50 reinforced concrete segmental lining. The depth of the tunnel crown is 16.99–25.40 m. The investigation data suggest that the caverns are the main dissolution phenomenon in this area, and most of them are located underneath the tunnel with varying depths. Most of the cavern accumulations are clayey soil of various colors or clayey soil mixed with gravel, and a few caves feature medium-dense grayish-yellow gravelly soil or gravelly soil. The majority of caves remain in a state of limited or absence of water, accordingly, the influence of karst water on shield tunnel construction at this location is comparatively negligible.

According to the investigation report, the strata traversed by the construction area are generally binary strata, principally divided into miscellaneous fill, plain fill and planting soil, with layer thickness of 0.30–6.40 m. The upper section is hard-plastic clay with gravel and hard plastic red clay, with top plate burial depth of 0.50–12.50 m. The upper section is hard-plastic ancient clay, with layer thickness of 1.40–17.60 m, and the depth of the top plate is 0.50–12.50 m. The lower half is clay with gravel and hard-plastic red clay, with layer thickness of 0.70–4.25 m. The bottom section is bedrock, containing Cretaceous-Lower Tertiary (K-E) chalky mudstone, Triassic tuff, and Permian tuff. Among them, the main physical and mechanical property parameters of each soil layer and bedrock in the research section are shown in Table 1. The report shows that the red clay is predominantly hard-plastic, and the local soil-rock bond surface is soft-plastic at the low concave area due to waterlogging, and the physical parameters are the same with the hard-plastic red clay after the high-pressure rotary pile reinforcement treatment. There is no adverse geological condition in this part after the treatment of soft-plastic red clay.

3. BUILDING THE FINITE ELEMENT MODEL

3.1. Model verification

According to the research by Mo Yangchun *et al.* [11, 14], it can be seen that the karst cave has a large influence on the plastic zone and displacement field of the rock and soil around the tunnel. In order to reduce the influence of the model size and boundary on numerical analysis results, the horizontal length of the model is 3–5 times the excavation depth, and the vertical length is 2–4 times the excavation depth. The length, width and height of the model is thus 162 m × 62 m × 62 m. Among these, normal constraints are applied to the bottom and side of the model accordingly, and the top surface is the free surface. Considering the average size of the cave in the selected part, the model simplifies the cave as an elliptical cylinder and the tunnel lining as a ring. At the same time, in order to decrease the mistake caused by too much mesh and the parameters, the model reduces the actual construction process and boundary conditions: it is assumed that a tunnel lining length (1.50 m) is excavated for each working condition, and the tunnel lining is activated at the same time. The first functioning condition corresponds to No. 1 tunnel lining, and so on. The inner diameter of tunnel lining is 5.50 m, the outer diameter is 6.20 m, and the thickness is 350.00 mm. In addition, the following assumptions are made: 1) the rock and soil layer is elastic-plastic material, which conforms to the Mohr-Coulomb elastic-plastic yield criterion; 2) tunnel lining and grouted body are elastic materials, which conform to the linear elastic yield criterion; 3) rock soil layer, tunnel lining and grouted body are homogeneous isotropic materials; 4) tunnel lining adopts a three-dimensional ring with uniform stiffness.

Table 1
Main physical and mechanical property parameters of each soil layer and bedrock

Materials	Natural gravity γ [kN·m^{-3}]	Cohesive force c [kPa]	Internal friction angle φ [°]	Poisson ratio μ	Compression modulus Es [MPa]
miscellaneous fill	19.6	5	19	0.20	5.0
plain fill	18.5	9	10	0.20	5.0
clay	19.5	40	16	0.35	16.4
soil-rock	20.2	42	18	0.35	19.0
red clay	21.5	37	18	0.30	25.0
limestone	25.6	40	24	0.35	46.0

The model tunnel lining is made of C50 concrete, and the grouted body is cementing mortar with parameters referring to C20 concrete. According to the construction plan, the cavern treatment in the analyzed section uses the slurry filling method, and the grouted body is regarded as the solid in the model for simulation. The material parameters of tunnel lining and grouted body are listed in Table 2.

Table 2
Material parameters of segment and grouting body

Materials	Natural gravity γ [kN·m^{-3}]	Poisson ratio μ	Elastic modulus E [MPa]
duct piece	24.0	0.30	34 500
grouted body	23.6	0.20	25 500

In the finite element simulation process, the initial stress calculation after grouting treatment of the cavern was carried out first, and then the shield excavation simulation was carried out to get the surface settlement cloud map. The results obtained from the simulation were compared with the actual measured data of the project. As the results in Fig. 1 show, the actual monitoring values and model values have the same trend with little difference, which proves it is feasible to use numerical simulation methods for analysis of the effect of the cavern on surface settlement.

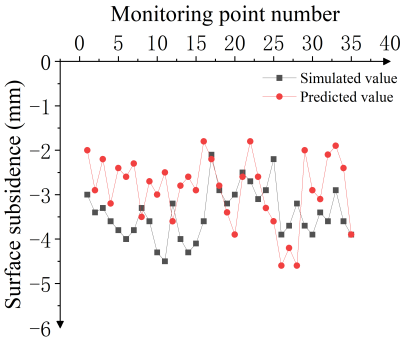

Fig. 1. Comparative map of surface subsidence

3.2. Model building

In practical engineering, due to the complicated geology of the karst regions and many influencing elements, it is usually necessary to analyze the common effect of multiple factors and to determine the correlation of multiple factors. However, too many design factors will substantially increase the number of required test groups and the computations quantity of the computer, thus this paper intercepts a portion containing a typical cavern (CK40+685.25–CK40+745.25) from the selected section to construct a finite element model. The length, width and height of the model are 60 m × 62 m × 62 m, and the cavern is simplified into a cylinder while the number of caverns is set to 1, and other parameters and assumptions are the same as above. The selected typical section model is shown in Fig. 2a. Vertical displacement constraints are applied to the bottom of the model, horizontal displacement constraints are applied to the sides, and no constraint is applied to the top surface (Fig. 2b). In order to genuinely replicate the actual construction process, the model sets up the tunnel excavation to proceed gradually (Fig. 2c). After calculation, maximum settlement of the ground surface following tunnel excavation is obtained.

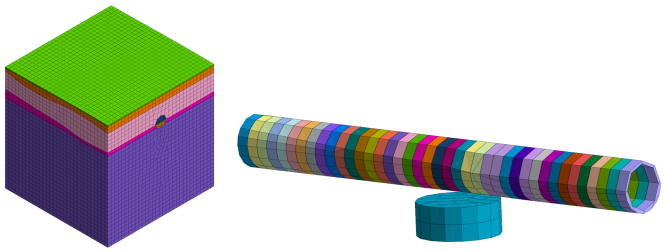

(a) Model grid

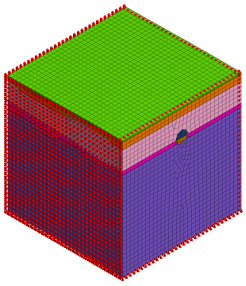

(b) Boundary constraint condition

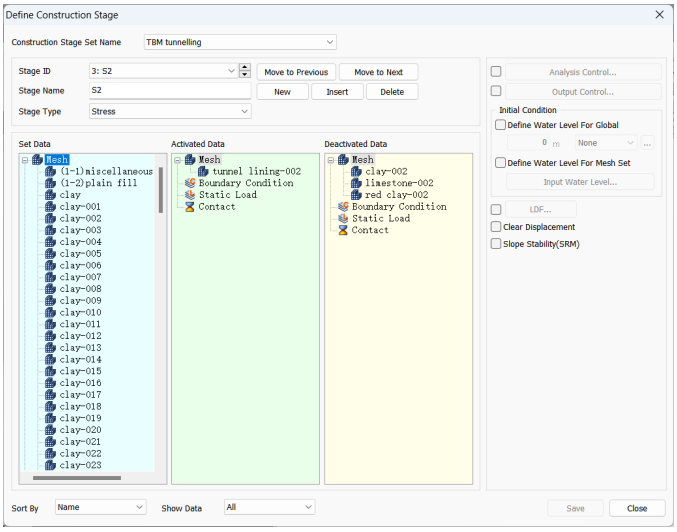

(c) Define construction stage

Fig. 2. Finite element calculation process

4. FINITE ELEMENT SIMULATION AND ANALYSIS

According to the research by Wang Xiangguo *et al.* [15–17], the affecting factors of the cavern on the TBM tunnel include predominantly the size of the cavern itself, the relative position of the cavern and the tunnel and water pressure of the cavern. The engineering research data prove that most of the caves in the selected study region are in the state of no water or little water, thus the influence of karst water can be neglected. Therefore,

this study primarily investigates the influence of five parameters – radius, height, vertical clearance between the karst cave and tunnel, horizontal clearance, and the angle between the tunnel axis and karst cave axis (referred to as "angle" hereinafter) – on maximum surface settlement, considering both treated and untreated karst conditions.

4.1. Gray correlation analysis

Gray system theory, a system science theory pioneered by Chinese researcher Deng Julong [18], is a regularly utilized study method for uncertain systems. Gray correlation analysis is one of the important research components of gray system theory, which can assess the correlation between factors by comparing the geometric similarity between the reference and comparison series. Even under the condition of limited data, it can effectively determine the degree of correlation between various changing factors and reference factors. The higher the correlation coefficient, the stronger the correlation, and vice versa.

4.1.1. Selection of test parameters

Although the number of sample size has no effect on the gray correlation analysis, it is desirable to secure more thorough data as much as it is feasible when designing the experiment. In this study, the data selection method in the orthogonal test was applied. The orthogonal experiment picks data according to the orthogonal table obtained from combinatorial mathematical theory, which is representative. A total of five parameters were selected in this investigation, and the L25(5^5) orthogonal table was used for data selection. The numbers of factors and levels in the orthogonal analysis are provided in Table 3, while the data collected from the MIDAS GTS simulation are shown in Table 4 and Fig. 3.

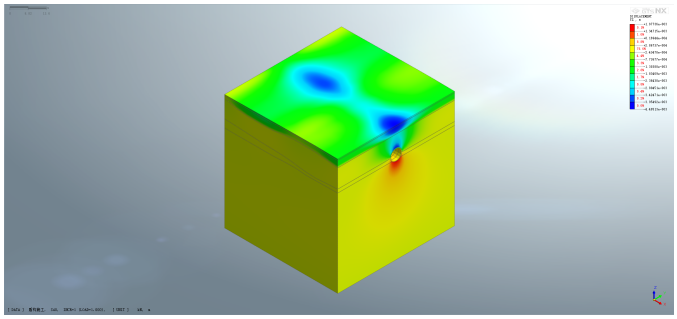

(a) Condition 1

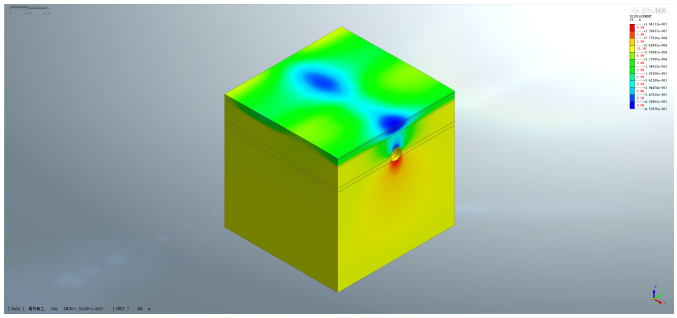

(b) Condition 5

Fig. 3. Surface subsidence displacement cloud map

Table 3
Number of factors and levels

Materials	Natural gravity γ [kN·m^{-3}]	Poisson ratio μ	Elastic modulus E [MPa]
duct piece	24.0	0.30	34500
grouted body	23.6	0.20	25500

Table 4
Finite element simulation results

Conditions	X_0 [mm]	X_0' [mm]	X_1 [m]	X_2 [m]	X_3 [m]	X_4 [m]	X_5 [°]
1	4.49	4.48	1.0	2.0	2.0	2.0	0
2	4.49	4.48	1.0	4.0	3.0	4.0	15
3	4.50	4.47	1.0	6.0	4.0	6.0	30
4	4.51	4.47	1.0	8.0	5.0	8.0	45
5	4.54	4.47	1.0	10.0	6.0	10.0	60
6	4.51	4.48	2.0	2.0	3.0	6.0	45
7	4.54	4.47	2.0	4.0	4.0	8.0	60
8	4.60	4.46	2.0	6.0	5.0	10.0	0
9	4.67	4.47	2.0	8.0	6.0	2.0	15
10	4.62	4.45	2.0	10.0	2.0	4.0	30
11	4.59	4.48	3.0	2.0	4.0	10.0	15
12	4.68	4.47	3.0	4.0	5.0	2.0	30
13	4.83	4.46	3.0	6.0	6.0	4.0	45
14	4.93	4.44	3.0	8.0	2.0	6.0	60
15	5.00	4.42	3.0	10.0	3.0	8.0	0
16	4.74	4.48	4.0	2.0	5.0	4.0	60
17	5.02	4.45	4.0	4.0	6.0	6.0	0
18	5.67	4.43	4.0	6.0	2.0	8.0	15
19	6.00	4.40	4.0	8.0	3.0	10.0	30
20	6.47	4.44	4.0	10.0	4.0	2.0	45
21	5.93	4.47	5.0	2.0	6.0	8.0	30
22	6.91	4.46	5.0	4.0	2.0	10.0	45
23	7.74	4.47	5.0	6.0	3.0	2.0	60
24	11.07	4.41	5.0	8.0	4.0	4.0	0
25	11.66	4.36	5.0	10.0	5.0	6.0	15

In the table, X_0 is the maximum surface settlement prior to cavern treatment; X_0' is the maximum surface settlement following cavern treatment; X_1 is the cave radius; X_2 is cave height; X_3 is the vertical clear distance between the cavern and the tunnel; X_4 is the horizontal clear distance between the cavern and the tunnel; and X_5 is the angle between the tunnel axis and karst cave axis, the same as below.

4.1.2. Calculation step

Gray correlation analysis starts with determining the reference sequence and the comparison sequence. According to Table 3, the five elements of the cave radius, cave height, vertical clear distance, horizontal clear distance and angle are identified as the comparison sequence, and maximum settlement of the ground surface is the reference sequence.

1. Let the reference sequence be X_0

$$X_0 = \{X_0(1), X_0(2), \cdots, X_0(n)\}. \tag{1}$$

2. Let the comparison sequence be X_i

$$X_i = \{X_i(1), X_i(2), \cdots, X_i(n)\} \quad (i = 1, 2 \cdots 5). \tag{2}$$

3. Dimensionless processing of data.

The selected reference series represent various physical meanings with considerable differences in magnitude and order of magnitude, which cannot be directly calculated and examined, thus the data need to be processed to eliminate the magnitude and make them comparable. The data of this test are all greater than 0 and the numbers are large, so they are handled using homogenization. The reference series and comparative series after processing are as follows:

$$Y_0 = \{Y_0(1), Y_0(2), \cdots, Y_0(n)\}, \tag{3}$$

$$Y_i = \{Y_i(1), Y_i(2), \cdots, Y_i(5)\} \quad (i = 1, 2, \cdots, 5). \tag{4}$$

In the formula: $Y_0 = \dfrac{X_0(n)}{\overline{X_0}}$, $Y_i = \dfrac{X_i(n)}{\overline{X_i}}$,

$$\overline{X_0} = \frac{1}{n}\left[X_0(1) + X_0(2) + \cdots + X_0(5)\right], \tag{5}$$

$$\overline{X_i} = \frac{1}{n}\left[X_i(1) + X_i(2) + \cdots + X_i(5)\right]. \tag{6}$$

4. Calculate the gray correlation coefficient $\xi_i(k)$

$$\xi_i(k) = \frac{\min\limits_i \min\limits_k \left|Y_0(k) - Y_i(k)\right| + \rho \max\limits_i \max\limits_k \left|Y_0(k) - Y_i(k)\right|}{\left|Y_0(k) - Y_i(k)\right| + \rho \max\limits_i \max\limits_k \left|Y_0(k) - Y_i(k)\right|}. \tag{7}$$

In the formula: $i = 1, 2, \cdots, 5$; $k = 1, 2, \cdots, n$; ρ is the resolution coefficient, and $\rho \in [0, 1]$. According to formula (7), it can be inferred that $\xi_i(k)$ is mainly affected by the maximum value when $|Y_0(k) - Y_i(k)| \gg |Y_0(k) - Y_i(k)|$, and all the correlation coefficients are close to 1, which is not credible. On the contrary, when $|Y_0(k) - Y_i(k)| \ll |Y_0(k) - Y_i(k)|$, the formula will lose the regulation effect on $\xi_i(k)$, and $\xi_i(k)$ is only affected by $|Y_0(k) - Y_i(k)|$, and it also does not have credibility. Therefore, this paper believes that selecting a moderate value ($\rho = 0.5$) can reduce the distortion effect caused by the maximum difference at two extreme levels, and thus improve credibility of the gray correlation coefficient.

5. Calculate the correlation R_i

$$R_i = \frac{1}{n}\sum_{k=1}^{n} \xi_i(k) \quad (i = 1, 2, 3, 4, 5). \tag{8}$$

4.1.3. Analysis of calculation results

Based on the above calculation steps, the two sets of data are calculated using MATLAB. The data in Table 4 are homogenized. Then the correlation between the radius, height, vertical clearance between the cavern and the tunnel, lateral clearance, and angle and maximum settlement of the ground surface are computed according to equation (1), and equation (2) correspondingly, and results are listed in Table 5.

Table 5
Gray correlation degree of each factor

Influencing factor	X_1	X_2	X_3	X_4	X_5
R_i	0.7810	0.7243	0.7228	0.6960	0.6428
R_i'	0.6104	0.6106	0.6670	0.6106	0.5341

Table 5 shows that, in the case of untreated cave, the influence of each factor on maximum surface settlement is ranked in the order of magnitude: radius R_1 > cave height R_2 > vertical clearance $R_3 > 0.7$ > horizontal clearance R_4 > angle $R_5 > 0.6$, which indicates that the influence of these factors on maximum settlement of the surface is relatively significant. Meanwhile, according to the detailed numerical study, the influence of the radius of the cavern is substantially bigger than those of the other factors. The influence of lateral clear distance and angle between the cavern and the shield tunnel is smaller than those of the other factors.

In the situation where the cave has been treated, the influence of each factor on maximum surface settlement is ranked in the order of magnitude: 0.7 > vertical clear distance R_3' > cave heightR_2' = lateral clear distance R_4' > radius R_1' > 0.6 > angle R_5'. It can be shown that after the treatment of the cavern, the influence of each factor on maximum surface settlement is greatly reduced as compared with the pre-treatment. According to the finite element simulation results, the maximum surface settlement value following cave treatment is in the interval of [4.36; 4.48], and the settlement value decreases while the value is more stable, which proves reliability of the gray correlation; it shows that cave treatment is effective in reducing maximum surface settlement, which is consistent with the conclusion of the study by Xie Haixu *et al.* [19].

For the untreated caverns, maximum surface settlement X_0 in Table 4 is divided into five groups according to the radius, and in order to reduce the influence generated by the large discrete nature of some data, the five groups of data are averaged and plotted on the graph according to the corresponding radius, and the plotted image is roughly showing a significant quadratic relationship, as presented in Fig. 4. Using Origin software for fitting, the following fitting formula is obtained:

$$X_0 = 0.16883X_1^2 + 3.80939. \tag{9}$$

The fitting degree of the obtained formula can be assessed using the determination coefficient R^2. R^2, which ranges from 0 to 1, is closer to 1 indicating a better fit. The determination coefficient

$R^2 = 0.70091$ shows that the correlation of the fitted formula is more significant and the assumption is more reasonable. The reason for the determination coefficient < 0.8 is evaluated as the usage of an orthogonal table to pick parameters in the software simulation, and multi-factor coupling influences the results. According to the distribution of data points and the fitted formula, it can be seen that within the selected range of the study, the positive correlation between maximum surface settlement and the cavern radius is significant, i.e. the larger the cavern radius, the larger the value of maximum surface settlement.

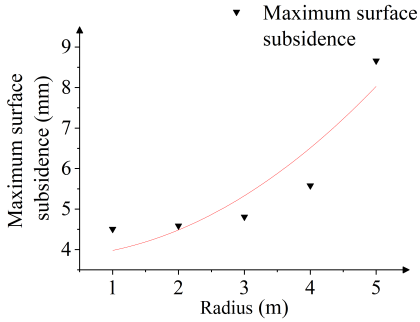

Fig. 4. Relationship between radius and maximum surface subsidence

Similarly, by grouping maximum surface settlement X_0 according to the other four factors, averaging the values and plotting the images, the relationship between maximum surface settlement and the other four factors can be determined in Fig. 4 with the fitting formulas (10)–(13). The determination coefficient is provided after the formulas.

$$X_0 = 0.216X_2 + 4.3324, \qquad R^2 = 0.95173, \tag{10}$$

$$X_0 = -0.0162X_3 + 5.6932, \qquad R^2 = 0.00255, \tag{11}$$

$$X_0 = -0.0692X_4 + 6.0436, \qquad R^2 = 0.27840, \tag{12}$$

$$X_0 = -0.2246X_5 + 6.0776, \qquad R^2 = 0.56900. \tag{13}$$

In Fig. 5d, to visualize the image, each unit of "1" in the horizontal coordinate is defined to represent 15°. From Fig. 5a, it can be observed that maximum surface settlement is positively connected with the height of the cavern; this is also substantiated by the relationship between maximum surface settlement and the height when the radius is the same in Table 4. The determination coefficients of formulas (11)–(13) are relatively small, indicating that maximum surface subsidence is primarily influenced by the radius and height of the karst cave, while other factors have minimal impact. The inability to control individual variables using the orthogonal analysis method resulted in less apparent regularity and poor fitting of some results. From the fitting formulas and Fig. 5, it can be shown that the vertical clear distance, horizontal clear distance and the angle of pinch are negatively connected with maximum surface settlement, which is consistent with the conclusions of the literature [20] study. This shows that the patterns obtained from formulas (11)–(13) are indeed correct.

In Table 4, the settlement values of untreated caves in the 24th and 25th conditions are increased considerably as compared to

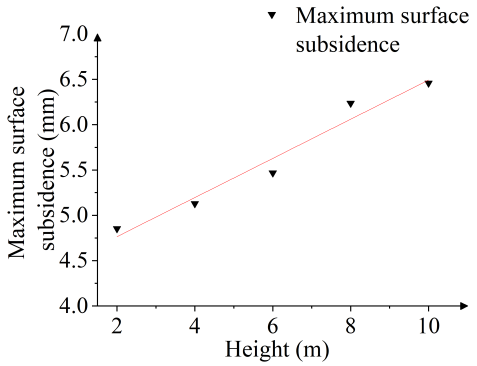

(a) Height

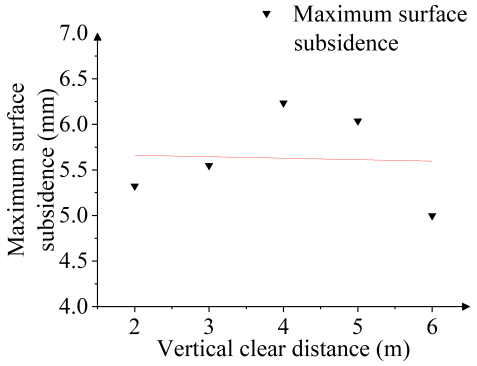

(b) Vertical clear distance

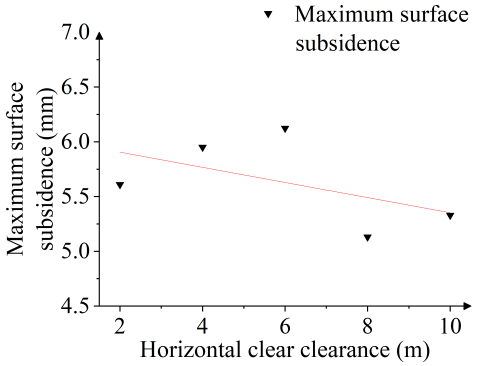

(c) Horizontal clear clearance

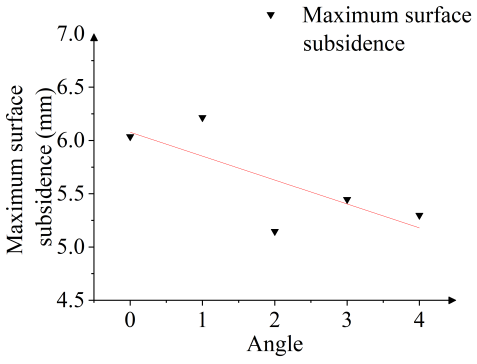

(d) Angle between the tunnel axis and karst cave axis

Fig. 5. Relationship between the factors of the karst cave and maximum surface subsidence

the preceding ones. Two anomalous conditions are analyzed, which are 5 m radius and 8 m height, and 5 m radius and 10 m height caverns, respectively. The tunnel diameter of the model established in this study is 6.2 m, and the heights of the two caverns are more than the tunnel diameter; and when the radius of the cavern is ≥ 4 m, maximum surface settlement increases significantly as compared with the radius of the smaller one, from which it is inferred that when the height of the cavern is larger than the diameter of the tunnel, and the cavern radius is larger than the radius of the tunnel, the influence of the cavern on maximum surface settlement will be enhanced significantly. In the actual project, we should pay more attention to similar situations and deal with them cautiously.

From Fig. 4 and Fig. 5a, it can be shown that the influence of the relationship between the radius and height of the cavern on maximum surface settlement coincides with the cylindrical volume formula $V = \pi R^2 h$. Combining them into the volume of the cavern, the conclusion is obtained which is compatible with that in the literature [20–22], i.e. the larger the cavern size (volume), the larger the surface settlement.

Table 6
Maximum surface subsidence difference

Conditions	1	2	3	4	5
subsidence difference [mm]	0.01	0.01	0.03	0.04	0.07
Conditions	6	7	8	9	10
subsidence difference [mm]	0.03	0.07	0.14	0.20	0.17
Conditions	11	12	13	14	15
subsidence difference [mm]	0.11	0.21	0.37	0.49	0.58
Conditions	16	17	18	19	20
subsidence difference [mm]	0.26	0.57	1.24	1.60	2.03
Conditions	21	22	23	24	25
subsidence difference [mm]	1.46	2.45	3.27	6.66	7.30

For the treated caves, the influence of each factor on maximum surface settlement is determined in the preceding section to be significantly reduced as compared with that before treatment, and the correlation is roughly 0.6. Table 6 shows the difference of maximum surface settlement before and after the treatment of the cavern, and it is found that when the radius of the cavern is ≥ 4 m and the height of the cavern is ≥ 6 m, the difference increases significantly, indicating that the treatment of the cavern with larger radius and height has a very obvious effect, and that the cavern with a diameter and height larger than the diameter of the tunnel needs to be properly handled in the actual project.

4.2. Multi-factor coupled modeling and validation

4.2.1. Multi-factor modeling

In the correlation study in Section 4.1.3, it is concluded that each factor of the untreated cavern has a relatively significant effect on maximum settlement of the surface, and there is a certain coupling between them, so the influence of each factor should be considered comprehensively in the establishment of the multi-factor model of maximum settlement of the surface.

For the case of untreated caverns, it is concluded in Section 4.1.3 that "the larger the size (volume) of the cavern, the larger the surface settlement", so the relationship between maximum surface settlement and the radius of the cavern is assumed to be a quadratic relationship (monotonically increasing in the domain of definition), and the relationship with height is assumed to be a linear relationship. The influence of the coupling relationship between the cavern radius and height on maximum surface settlement can be assumed as formula (14):

$$X_0 = \left(AX_1^2 + B\right)(CX_2 + D). \tag{14}$$

In the formula: X_0–X_2 corresponds to Table 4, respectively, while maximum settlement, radius and height of the surface, A–D is the coefficient to be determined.

There is a negative correlation between the cavern and the vertical clear distance, horizontal clear distance and angle of the tunnel, but by the influence of multi-factor coupling, the degree of correlation is weaker, and its correlation degree calculated by the gray correlation analysis method is also smaller than the radius and height; therefore, it is assumed that the relationship between these three factors and maximum subsidence of the ground surface is a linear relationship, to obtain the full-factor model form assumed as formula (15):

$$X_0 = \left(AX_1^2 + B\right)(CX_2 + D)(EX_3 + F)(GX_4 + H)(LX_5 + J) + K. \tag{15}$$

In the formula: X_0–X_5 corresponds to Table 4, respectively, maximum settlement of the surface, radius, height, vertical clearance, lateral clearance and angle; A–K is the coefficient to be determined.

According to formula (15) and the data in Table 4, using Origin for fitting, the determination coefficient of the fitting formula can be obtained as $R^2 = 0.85258$, from which can be seen that the correlation of the obtained model is very significant, and the assumption is more reasonable. The specific mathematical model can be seen in formula (16). From the resulting formula (16), it can also be shown that vertical clear distance, lateral clear distance and the angle of the maximum impact of surface settlement are much smaller than the radius and height, indicating that the prior assumptions are valid.

$$X_0 = \left(0.15488X_1^2 - 0.89889\right)(0.16081X_2 - 0.10507)(0.00911X_3 + 0.33078)(-0.03148X_4 + 0.77125)(-0.06411X_5 + 7.28382) + 4.761. \tag{16}$$

4.2.2. Multi-factor model validation

1. Finite element verification

All the operating condition parameters are inserted into formula (16) for computation, and the predicted values are compared and analyzed with the software simulation values, while

the results are presented in Fig. 6. The predicted values derived by formula (16) are quite near to the simulated values of MIDAS, which shows that the obtained formula (16) can accurately depict the link between the factors of the cavern and the maximum settlement of the ground surface.

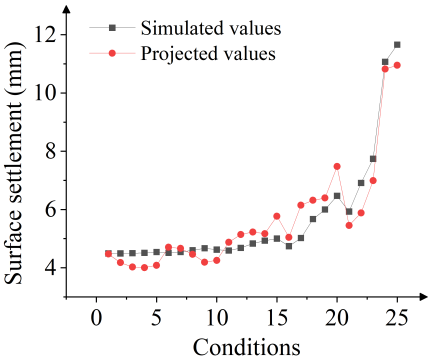

Fig. 6. Simulated value and predicted value

After calculation, it can be observed that the ratio of the simulated value to the predicted value has a mean value $\mu = 1.00431$, a standard deviation $\sigma = 0.09845$, and a coefficient of variation $\delta = 0.09802$, which indicates that the above computational model has a high prediction accuracy and good applicability.

2. Engineering verification

Verified with YC794, YC796, YC798 caves, cave-related characteristics and settlement values are listed in Table 7, in which the angle between the cave and the tunnel are 0°, and the conversion radius is the radius of converting elliptical caves into circular caves of equal area. The prediction is closer to the engineering monitoring, and the error is mostly attributable to the following aspects: 1) The model has simplified the stratigraphic parameters, and the model can only divide the approximate range, which cannot accurately reflect the actual situation, and does not take into account the factor of groundwater; 2) Underground caverns have different shapes, which are difficult to be explored, and the model cannot accurately reflect the real situation, while the shape of the caverns has a significant effect on maximum settlement of the ground surface; [22] 3) In addition to the error between the finite element model and the actual situation, there is also a certain error between the fitted formula and the finite element model, and the superposition of the two may produce a large error.

5. CONCLUSIONS

Based on three-dimensional finite element simulation, this paper investigates the influence of the parameters of the cavern under the tunnel on the maximum settlement of the ground surface when the TBM tunnel passes through the karst area with the background of an interval project of the Wuhan Metro. The following conclusions are drawn:

1. When the cavern is not treated, the degree of influence of each factor on maximum settlement of the ground surface is as follows: radius R_1 > cavern height R_2 > vertical clear distance R_3 > 0.7 > horizontal clear distance R_4 > angle R_5 > 0.6; among them, the radius and height of the cavern occupy a dominant position. The radius and height of the cavern are positively correlated with maximum surface settlement; the vertical clear distance, lateral clear distance, and the angle of pinch are negatively correlated with maximum surface settlement, and their effects on the settlement are very weak as compared with the radius and height. After the cave treatment, the sequence is: 0.7 > vertical clearance R'_3 > cave height R'_2 = lateral clearance R'_4 > radius R'_1 > 0.6 > angle R'_5; the influence of vertical clearance on maximum ground surface settlement is greatest, but compared with before treatment, its influence is significantly lower.
2. Grouting of the cavern can significantly reduce the impact of the cavern on maximum settlement of the surface, thereby minimizing surface settlement. For caverns with a radius greater than the tunnel radius and a height greater than the tunnel diameter, careful consideration and proper treatment should be employed. For small caverns with a radius smaller than the tunnel radius and a height smaller than the tunnel diameter, the impact of surface settlement differs little, and the decision to treat or not depends on the project's specific experience and status.
3. The influencing factors of surface settlement caused by karst caves are interdependent, and it is not appropriate to analyze a single factor independently in practical engineering scenarios. The multi-factor calculation model for maximum surface settlement presented in this study offers high prediction accuracy and excellent applicability. This model may serve as a valuable reference and provide research insights for the prediction and assessment of maximum surface settlement in similar projects.
4. This study investigates the influence of various karst cave parameters on maximum surface settlement, using a spe-

Table 7
Karst cave parameters

Cave number	Long axis × short axis [m]	Conversion radius [m]	Height [m]	Vertical clear distance [m]	Horizontal clear clearance [m]	Predicted settlement [mm]	Actual settlement [mm]
YC794	1.85 × 0.705	0.589	4.5	9.7	2.2	3.64	3.40
YC796	1.425 × 0.76	0.52	6.4	3.3	1.41	3.25	3.10
YC798	3.32 × 2.00	1.29	8.8	9.4	0	2.80	2.40

cific subway project in Wuhan as the background, and the values of each parameter are also confined to a specified range. Therefore, the predicted values derived from the prediction model in this study should be used as references only. For different projects, more influencing factors need to be considered, and more comprehensive research needs to be conducted in combination with the actual situation.

REFERENCES

[1] D. Ford, "Jovan Cvijić and the founding of karst geomorphology," *Environ. Geol.*, vol. 51, no. 5, pp. 675–684, 2007, doi: 10.1007/s00254-006-0379-x.

[2] G. Chunqing, W. Li, and W. Hongtao, "The research of karst ecological geology in China," *Ecol. Environ.*, vol. 2, pp. 275–281, 2005, doi: 10.16258/j.cnki.1674-5906.2005.02.030.

[3] Z. Mingjie, A. Jianhua, L. Xuhua, and W. Biao, "Model testing research on influence of karst cave size on stability of surrounding rockmasses during tunnel construction," *Chin. J. Rock Mech. Eng.*, vol. 2, pp. 213–217, 2004.

[4] Y. Fang, C. He, A. Nazem, Z.G. Yao, and J. Grasmick, "Surface settlement prediction for EPB shield tunneling in sandy ground," *KSCE J. Civil Eng.*, vol. 21, no. 7, pp. 2908–2918, 2017, doi: 10.1007/s12205-017-0989-8.

[5] L. Li, S. Sun, J. Wang, W. Yang, S. Song, and Z. Fang, "Experimental study of the precursor information of the water inrush in shield tunnels due to the proximity of a water-filled cave," *Int. J. Rock Mech. Mining Sci.*, vol. 130, p. 104320, 2020, doi: 10.1016/j.ijrmms.2020.104320.

[6] L. Shucai, W. Kang, L. Liping, Z. Zongqing, S. Shaoshuai, and L. Shang, "Mechanical mechanism and development trend of water-inrush disasters in karst tunnels," *Chin. J. Theor. Appl. Mech.*, vol. 49, no. 1, pp. 22–30, 2017, doi: 10.6052/0459-1879-16-345.

[7] B, Zou, M. Chibawe, B. Hu, Y. Deng, "A comparative analysis of artificial neural network predictive and multiple linear regression models for ground settlement during tunnel construction," *Arch. Civ. Eng.*, vol. 69, no. 2, pp. 503–515, 2023, doi: 10.24425/ace.2023.145281.

[8] W. Bogusz, T. Godlewski, and A. Siemińska-Lewandowska, "Parameters used for prediction of settlement trough due to TBM tunnelling," *Arch. Civ. Eng.*, vol. 67, no. 4, pp. 351–367, 2021, doi: 10.24425/ace.2021.138504.

[9] T. Daiming, Q. Taiyue, and M. Yangchun, "Numerical analysis and research on surrounding rock stability of lateral karst cave tunnel," *Chinese J. Rock Mech. Eng.*, vol. 28, no. A2, pp. 3497–3503, 2009, doi: 10.3321/j.issn:1000-6915.2009.z2.031.

[10] Y. Jiemin, "Numerical Simulation of the Stability of Subway Tunnel in Karst Regions," M.Sc. thesis, South China University of Technology, Guangzhou China, 2011.

[11] M. Yangchun and Z. Xiaojun, "Numerical simulation analysis on surrounding rock deformation characteristic of tunnel with karst cave beside," *Hydrogeol. Eng. Geol.*, vol. 35, no. 2, pp. 30–34, 2008.

[12] L. Daoyan, X. Jianbin, L. Zhong, and S. Xiaohai, "Numerical Analysis on Influence of Concealed Karst Caverns upon Stability of Metro Shield Tunnel," *Tunnel Constr.*, vol. 40, no. A2, pp. 151–160, 2020, doi: 10.3973/j.issn.2096-4498.2020.S2.020.

[13] Z. Fang *et al.*, "The Influence of Different Karst Cave Filling Material Strengths on Stratum Stability During Shield Tunneling," *Geotech. Geolog. Eng.*, vol. 41, no. 2, pp. 1309–1323, 2023, doi: 10.1007/s10706-022-02337-w.

[14] L. Yuanhai, Y. Su, Y. Jun, and G. Kunrong, "Influence of a Large Karst Cave on Rock Mass Stability during Tunnelling," *Mod. Tunn. Technol.*, vol. 53, no. 4, pp. 52–60, 2016, doi: 10.13807/j.cnki.mtt.2016.04.008.

[15] W. Xiangguo, "Sensitivity Analysis of Effect of Different Cavern Conditions on Excavation of Long-Span Tunnels," *J. Chin. Foreign Highway*, vol. 41, no. 4, pp. 252–255, 2021, doi: 10.14048/j.issn.1671-2579.2021.04.050.

[16] G. Rui, L. Chen, Z. Bo, and S. Bo, "Impact of Karst Cave on Tunnel Structure Deformation and Stress:a Case Study of the Dafang Tunnel," *Sci. Technol. Eng.*, vol. 20, no. 9, pp. 3770–3777, 2020.

[17] L. Ting, G. Xin, H. Fan, J. Yanfei, H. Jinlong, and L. Lele, "Numerical Analysis of Influence of Water Pressure of Overlying Karst Cave on Tunnel Water Inrush," *Tunnel Constr.*, vol. 37, no. 2, pp. 167–172, 2017, doi: 10.3973/j.issn.1672-741X.2017.02.007.

[18] Deng Julong, *Basic Method of Gray System*. 1987.

[19] X. Haixu and C. Rong, "Influence of Grouting Reinforcement of Karst Caves on Subway Shield Tunnel Construction," *J. Northeast Electr. Power Univ.*, vol. 41, no. 6, pp. 120–128, 2021, doi: 10.19718/j.issn.1005-2992.2021-06-0120-09.

[20] C. Binghua, C. Deshan, F. Xiaola, and L. Zhongchao, "Study on Surface Deformation Pattern Caused by Small Shield Tunneling in Complex Strata in Karst Area of Wuhan," *Safety Environ. Eng.*, vol. 27, no. 1, pp. 69–74, 2020, doi: 10.13578/j.cnki.issn.1671-1556.2020.01.011.

[21] G. Xiaogan, "Study on the influence of hidden karst cave on tunnel surrounding rock stress and surface settlement," *Eng. Mach. Maint.*, vol. 1, pp. 67–69, 2023, doi: 10.3969/j.issn.1006-2114.2023.01.022.

[22] G. Yan, W. Xiaodong, and T. Jiayi, "Analysis and prediction of the influence of underground karst cave spatial morphology on land subsidence based on machine learning," *Acta Scientiarum Naturalium Universitatis Sunyatseni*, vol. 62, no. 2, pp. 83–92, 2023, doi: 10.13471/j.cnki.acta.snus.2022d019.